Received: 25 September 2020 | Revised: 2 December 2020 | Accepted: 6 January 2021

DOI: 10.1002/asl.1025

RESEARCH ARTICLE

Atmospheric Science Letters RMetS

Impacts of aerosols produced by biomass burning on the stratocumulus-to-cumulus transition in the equatorial Atlantic

Osinachi F. Ajoku[1,2] | **Arthur J. Miller**[1] | **Joel R. Norris**[1]

[1]Scripps Institution of Oceanography, University of California, San Diego, La Jolla, California

[2]National Center for Atmospheric Research, Boulder, Colorado

Correspondence
Osinachi F. Ajoku, Scripps Institution of Oceanography, University of California, San Diego, 9500 Gilman Dr., La Jolla, CA 92093, USA.
Email: oajoku@ucar.edu

Funding information
National Science Foundation, Grant/Award Numbers: OCE1419306, OCE1600283; National Science Foundation Graduate Research, Grant/Award Number: DGE-1650112

Abstract

The impact of aerosols produced by biomass burning on the stratocumulus-to-cumulus transition (SCT) in the equatorial Atlantic is studied using satellite-based and reanalysis data for the month of June. The month of June is highlighted because it represents monsoon onset as well as the largest sea surface temperature gradient in the summer, which is the peak season of tropical African biomass burning. Boundary layer deepening and increasing temperatures put the location of the SCT within the Gulf of Guinea. Satellite retrievals indicate that the bulk of aerosols occur near 1,500 m in altitude, either above or below the boundary layer depending on latitudinal position. Changes in smoke loading over the Gulf of Guinea due to greater transport from southern Africa leads to increases in low-level cloud cover above cloud decks and decreases when mixed within the boundary layer. Further south, we find significant changes to temperature, cloud top height, tropospheric stability and moisture availability near maximum aerosol loading. In addition, changes in vertical velocity during dirty conditions further reinforce changes in tropospheric stability. These effects combine to shorten the SCT in space during increased aerosol loading episodes.

KEYWORDS

aerosol radiative effects, lower tropospheric stability, stratocumulus-to-cumulus transition

1 | INTRODUCTION

Aerosols alter earth's radiation budget in three different ways, all of which can contribute to changes in cloud properties. The aerosol direct effect describes how aerosols impact the planetary energy balance through the absorption and scattering of incoming radiation (Haywood and Boucher, 2000; Ramanathan *et al*., 2001). Also, aerosols can influence cloud droplet size and consequently the likelihood of coalescence and the accumulation of liquid water and ice in clouds, thus altering cloud albedo and lifetime (Albrecht, 1989; Ferek *et al*., 2000; Ghan *et al*., 2012). This method is called the "aerosol indirect effect." Lastly, solar absorbing aerosols such as black carbon can alter heating rates, the vertical temperature profile and atmospheric stability, which can lead to

cloud adjustments. The radiation flux associated with this adjustment is termed the aerosol "semi-direct effect" (Hansen *et al*., 1997).

Differential heating on the earth's surface sets up regions with considerable meridional sea surface temperature (SST) gradients. In addition, locations with eastern boundary currents that transport cooler waters equatorward coupled with large-scale subsidence are dominated by persistent stratocumulus decks (Klein and Hartmann, 1993). As these decks follow the mean trade wind circulation equatorward, the cloud regime transitions from predominantly stratocumulus to trade cumulus (Bretherton, 1992; Bretherton and Wyant, 1997; Bretherton *et al*., 1999; Teixeira *et al*., 2011). A better understanding of this stratocumulus-to-cumulus transition (SCT) is important for modeling cloud interactions in a changed climate. As tropical regions are projected to expand under various modeled scenarios, so will corresponding subtropical dry zones which heavily influence the location of persistent stratocumulus decks (Allen and Ajoku, 2016). In terms of Hadley circulation, the subsiding portion coincides with persistent stratocumulus decks and thus a change in location and/or strength will impact the location of the SCT.

Factors that may potentially influence this transition have been studied using both observations (Albrecht *et al*., 1995; Wood *et al*., 2018; Albrecht *et al*., 2019) and model simulations (Sandu and Stevens, 2011; Chung *et al*., 2012). The major factors controlling cloud coverage and structure in these transition regions are lower tropospheric static stability (LTS) (Wood and Bretherton, 2006) and the typical advection of a cloud system over increasing SST. Specifically, increases in LTS create a stronger cap of the planetary boundary layer, allowing for greater low-level cloud coverage and hindering deep-cloud formation. The abovementioned cloud advection leads to larger surface latent heat fluxes, buoyancy fluxes and boundary layer deepening.

Satellite observations have been used to understand the influence of smoke aerosols on boundary layer clouds in the southeastern Atlantic (Painemal *et al*., 2014; Diamond *et al*., 2018). The consensus from such studies is that the location of the smoke layer relative to the cloud deck ultimately determines the resulting effect. When smoke resides above the cloud deck, there tends to be a strengthening of the inversion layer, increasing the cloud fraction and cloud radiative effect whereas smoke within the boundary layer leads to decreased the cloud fraction and increase the temperature within the boundary layer (Johnson *et al*., 2004; Wilcox, 2010; 2012).

There have been few studies that look into how smoke aerosols may impact the SCT (Sandu and Stevens, 2011; Terai *et al*., 2014; Painemal *et al*., 2015; Zhou *et al*., 2015; Yamaguchi *et al*., 2017) and fewer studies that used observations over the Atlantic Ocean. The Atlantic Stratocumulus Transition Experiment-ASTEX (Albrecht *et al*., 1995) conducted in 1992 resulted in data leading to a coherent understanding as well the first measurements of its kind for cloud microphysical properties in the SCT of the northeastern subtropical Atlantic but did not investigate the impact of smoke aerosols. In the southeastern subtropical Atlantic, there have only been a few studies solely looking at how aerosols may impact the during peak biomass burning season. The ORACLES campaign looks into aerosol–cloud interactions over the southeast Atlantic throughout the majority (August 2017, September 2016 and October 2018) of the biomass burning season (Zuidema *et al*., 2016; Cochrane *et al*., 2019; Pistone *et al*., 2019). CLouds and Aerosol Radiative Impacts and Forcing for Year 2017 (CLARIFY-2017) aimed to better represent the radiative and microphysical properties of stratocumulus clouds as they transition to cumulus clouds (Haywood et al., 2021).

Some studies that use large-eddy simulations (LES) to better understand this phenomenon (Yamaguchi *et al*., 2015; Zhou *et al*., 2017) incorporate observed data from the northeastern subtropical Pacific and knowledge of smoke aerosols from active fires interacting with stratocumulus clouds off the coast of Southern Africa. Both studies find evidence of aerosols impacting the SCT but through contrasting mechanisms and end results. Yamaguchi *et al*. (2015) attribute a delay of the SCT to increased LTS due to aerosol heating above the cloud layer, while Zhou *et al*. (2017) find a hastened transition due to increased cloud droplet number concentration and cloud water evaporation. Unlike these previous studies, we will examine SST, aerosol and meteorological conditions from observations and reanalysis within the equatorial Atlantic.

The scientific questions motivating this study are:

1. Can we clearly see a SCT region where biomass burning aerosol emissions impact low-level cloud fraction?
2. What are the important mechanisms by which biomass burning aerosols can possibly impact the spatial structure of the SCT?

Knowing that these transitions occur in all four subtropical ocean basins, not many locations can satisfy the added component of solar-absorbing aerosols (black carbon) being present. We have located a region in the equatorial Atlantic with cloud types transitioning from stratocumulus to trade cumulus and even deep convective cumulonimbus that have the potential to be influenced by local smoke aerosol emissions during the West African monsoon season. This study can be

important for designing future field campaigns and testing global climate models (GCMs) abilities to simulate the SCT.

2 | DATA SOURCES AND METHODS

Data analysis is conducted for June, representing monsoon onset as well as the establishment of a cold tongue in the eastern equatorial Atlantic Ocean. This cold tongue, located ~2°S–7°S, strengthens the capped stratocumulus deck leading to a much sharper transition. In addition, the intertropical convergence zone (ITCZ) migrates northward, intensifying trade winds and we identified June as having the largest meridional SST gradients among summer months. Our study region comprises of the boundary between 15°N–15°S and 10°W–10°E. The longitudinal boundaries in Figure 1a reflect the area used for zonal averaging. Also, it should be noted that SSTs decrease 2°C in the Gulf of Guinea (GoG) from the beginning to end of June. Our GoG study region is defined here to be between 0°N–5°N and 10°W–10°E. In order to prevent potential biases, SST and cloud data used in this study are detrended by the mean monthly June trend to remove variability arising solely from the seasonal cycle. In order to determine the impact of smoke aerosols on cloud structure daily averaged data are used in this study (with the exception of aerosol extinction). Higher temporal resolution is important for resolving synoptic-scale and mesoscale meteorological processes that otherwise may not be captured on monthly timescales.

A detailed description of daily aerosol from Modern-Era Retrospective analysis for Research and Applications, Version 2 (MERRA-2), precipitation from Global Precipitation Climatology Project. Version 1.3 (GPCP 1.3) and Clouds and Earth's Radiant Energy System (CERES) cloud data sources as well as how composite and statistical analysis for dirty and clean aerosol days are used in this study can be found in Ajoku *et al.* (2019). In brief, box average aerosol values over our GoG region were calculated and divided into pentiles. Calendar dates associated with the upper/lower 20% of values were used to create dirty/clean days composites. Aerosol data are based on a version of the NASA Goddard Earth Observing System version 5 (GEOS5) model that is radiatively coupled to the Goddard Chemistry, Aerosol, Radiation, and Transport (GOCART) aerosol module and includes assimilation of observations from satellites. In addition, level 3 aerosol angstrom exponent's over both ocean and land are obtained from the Visible Infrared Imaging Radiometer Suite (VIIRS) in daily format at 1° × 1° horizontal resolution for available years that overlap with this study (2013–2015). This product uses a Deep Blue

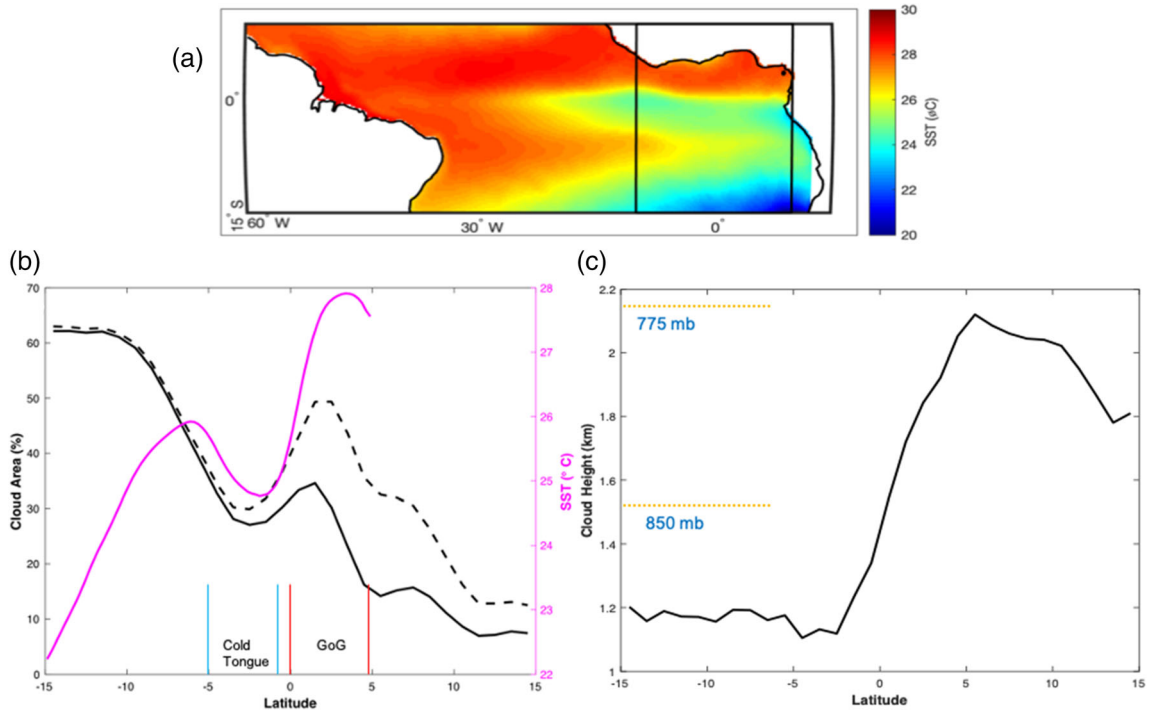

FIGURE 1 (a) Climatological June SST, (b) zonally averaged low cloud area fraction and SST and (c) corresponding cloud top height for the years 2003–2015. The black lines in (a) represents longitudinal boundaries used to average the data in (b) and (c) as well as subsequent figures. Dashed black lines in (b) represent cloud area fraction accounting for obscuration from high level clouds

(DB) algorithm over land and Satellite Ocean Aerosol Retrieval (SOAR) algorithm over ocean to determine atmospheric aerosol properties for daytime cloud-free scenes (Sayer *et al*., 2018). Although this product is limited to cloud-free scenes, Shinozuka *et al*. (2020) shows that aerosol optical depth (AOD) above low-level clouds is similar to adjacent clear skies in the southeast Atlantic. In addition, instantaneous 3-hourly data products on a 1.25° × 1.25° resolution were obtained for zonal, meridional and vertical wind speeds, cloud fraction, liquid cloud water content and temperature from MERRA-2 reanalysis (https://disc.gsfc.nasa.gov/datacollection/MAI3CPASM_5.2.0.html). The MAI3CPASM data product contains two-dimensional and three-dimensional fields outputted to 42 pressure levels. Temperature data produced by MERRA-2 are compared with data retrieved from the European Centre for Medium-Range Weather Forecasts (ECMWF) reanalysis product (Berrisford *et al*., 2011).

High-resolution (0.25° × 0.25°) daily SST data are provided by the National Oceanic and Atmospheric Administration's (NOAA) Earth System Research Laboratory (ESRL) Physical Sciences Division (Reynolds *et al*., 2007). NOAA's 0.25° daily Optimum Interpolation Sea Surface Temperature (OISST) data are compiled from observational platforms taking into account bias adjustments.

Monthly smoke aerosol extinction coefficients are acquired from NASA's Cloud-Aerosol Lidar and Infrared Pathfinder Satellite Observation (CALIPSO) platform for the years 2003–2015 using the Cloud-Aerosol Lidar with Orthogonal Polarization (CALIOP) instrument. CALIPSO lidar level 3 aerosol data product reports monthly mean profiles of aerosol optical properties on a 2° × 5° spatial grid (Winker, 2015) and 60 m resolution in the vertical direction. We use monthly data because the return time between overpasses is too long at daily intervals. Satellite imagery representing cloud and aerosol types within our study region are obtained from NASA's Worldview.

3 | RESULTS

3.1 | Study region overview

For the month of June, climatological conditions in the Eastern equatorial Atlantic are excellent for studying the SCT. Between the ITCZ migration and trade wind intensification, a large, meridional SST gradient sets up a corresponding cloud structure aloft (Figure 1a). Starting in the southern subtropical Atlantic moving equatorward, we see an inverse relationship between increasing SST and decreasing low-level cloud fraction (Figure 1b). Of particular interest, we notice two locations where cloud fraction decreases 50% (7°S–3°S and 1°N–5°N). We note that this decrease is not as pronounced when accounting for obscuration from high-level clouds. We designate the SCT as the location where SSTs and low clouds decrease simultaneously, which occurs in our datasets at roughly ~7°S. Between 5°S and 10°S, satellite imagery provided by MODIS captures smoke aerosols residing above cumulus clouds (Figure 2). Within the Gulf of Guinea (GoG), we examine the structure of cloud top height and find a ~700 m increase (Figure 1c) in the same location that the cloud fraction decreases. We assume this is where the boundary layer deepens due to increasing SST in GoG.

3.2 | Aerosol–low cloud–SST feedback

In order to understand aerosol–cloud interactions, first we must understand where biomass burning aerosols are located. June climatological AOD and 850 hPa winds (Figure 3a) show that, on average, aerosols advected over the GoG are due to seasonal trade winds on the African continent. In addition to total AOD, aerosol angstrom exponents at 532 nm obtained from satellite observations validate that the majority of particulates in our region are in the fine mode. Fine-mode aerosols are shown in Figure 3b through solid contour lines (angstrom exponent values greater than 1). It is essential to differentiate between fine and coarse mode aerosols to understand which may be influencing radiation and cloud microphysical properties. Fresh biomass burning produces aerosols that are highly absorptive and of the fine mode; thus, angstrom exponents are used to differentiate between these and other nonabsorptive aerosol species over the ocean (e.g., sea spray and dust). Long-term monthly-mean vertical smoke aerosol extinction coefficient profiles for the month of June representing locations in our study region are shown in Figure 4a. We see the largest values at 4°S and the equator at an altitude just below 1,500 m. This extinction maximum occurs above the low cloud top height (Figure 1c). Further north, we notice decreases in mean extinction as aerosols enter the boundary layer. Regardless of latitudinal location, values taper toward 0 near 5.5 km. Figure 4b shows that most of the smoke along the 0 longitude is located between 1,000 and 3,000 m specifically where AOD anomalies exceed 0.1 (~25% of the monthly mean) on dirty and clean days (Figure 3c,d). On average, the bulk of smoke aerosols between 0°S and 4°S are located above the boundary layer as evidenced by average cloud top height (Figure 1c) and throughout the lowest 5 km of the troposphere elsewhere.

During dirty biomass burning episodes, we find evidence of increased low cloud fraction specifically within

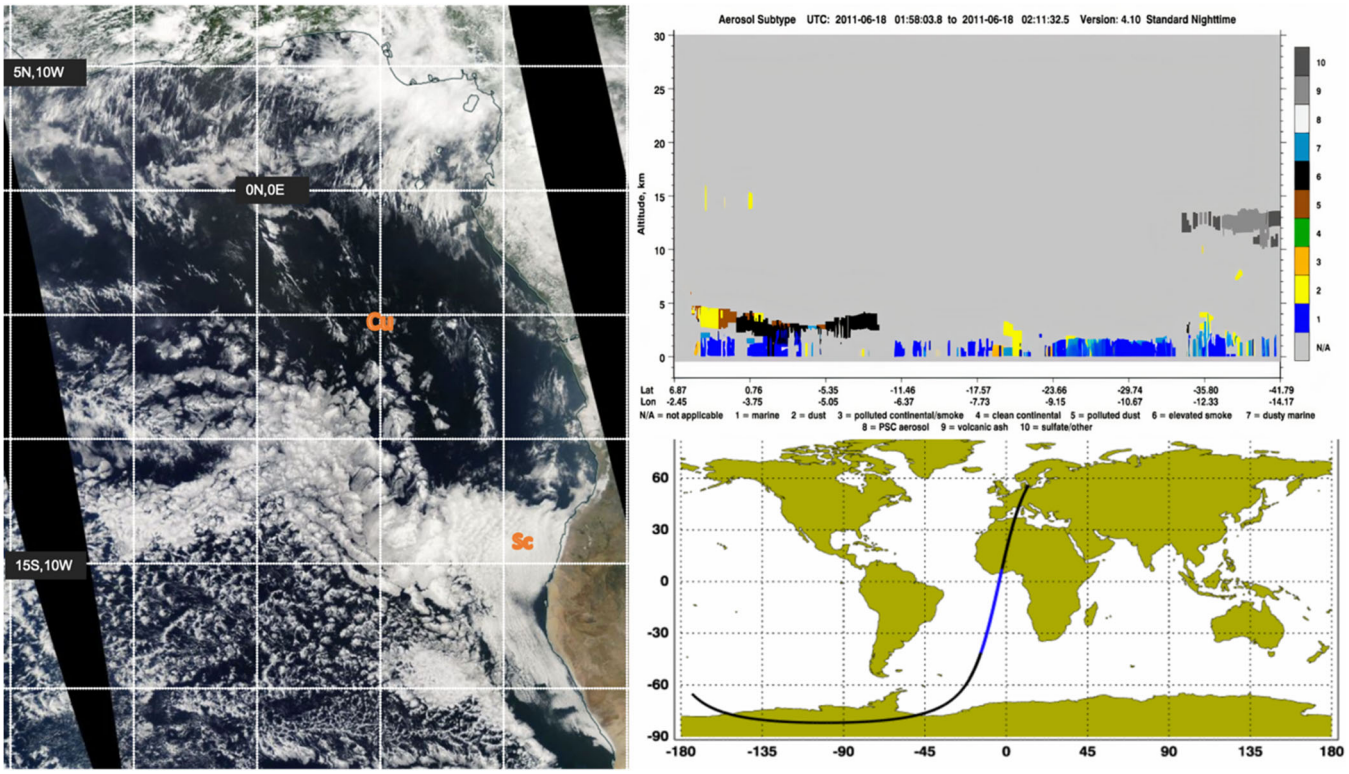

FIGURE 2 Satellite view on June 18, 2011 of stratocumulus and cumulus clouds within the equatorial Atlantic obtained from MODIS (left) with labels for each type. Text boxes reference the coordinates for selected graticules. Profile (top right) taken along satellite tract (bottom right) highlighted in blue

the equatorial Atlantic cold tongue zone and within the area where maximum aerosol loading occurs (Figure 5a). As low cloud fraction increases, it is possible the amount of shortwave radiation reaching the ocean surface diminishes as is reflected by changes in SST. However, we find positive low cloud fraction anomalies close to where cloud top heights reach a minimum in the cold tongue (Figure 1b). Figure 4a (black line) shows that the bulk of smoke aerosols resides above this height (~1,150 m) and Figure 6a shows that cloud top heights decrease during dirty days, although from 2°S to 15°S. As stated earlier, the location of smoke relative to a cloud deck determines the resulting aerosol–cloud interaction. Smoke residing above cloud decks in the Atlantic cold tongue lead to positive low cloud fraction anomalies during dirty days (Wilcox, 2010; 2012). The opposite response occurs during clean episodes, with low cloud fraction (Figure 5b) and increased cloud top height (Figure 6a).

3.3 | Stability versus moisture aloft

Yamaguchi *et al.* (2015) find that smoke aerosols delay the SCT by suppressing precipitation when in contact with clouds. In accordance with this study and others that look at LTS as a controlling factor for low cloud amount within SCT regions (Wood and Bretherton, 2006; Sandu and Stevens, 2011), we examined changes in potential temperature (θ) profiles and cloud top height anomalies (Figure 6a,b). Here, we can clearly see the effects of anomalous smoke loading on atmospheric stability. During dirty smoke episodes, we find significant decreases (25–100 m) in low-level cloud top height from the cold tongue southward (Figure 6a) and opposing increases during clean conditions. By analyzing θ anomalies along the 0 longitude transect, we can infer where aerosols impact stability within the lower troposphere (Figure 6b). As expected, the largest response occurs near 850 hPa, which corresponds to ~1,500 m above sea level (Figure 1c). In the Tropics (10°S and 4°S), we find the largest changes in cloud height and θ anomalies although smoke aerosol extinction values do not vary much between 750 and 4,000 m. In addition, we find notable changes in vertical velocity (Figure S1, Supporting Information) ~850 mb where the bulk of absorbing aerosols reside (Figure 4). The highly absorptive, fine mode aerosols residing above reflective stratocumulus decks aid to increase LTS in this transition region (Wood and Bretherton, 2006). Further north, these changes are less pronounced. We note significant cooling near the surface

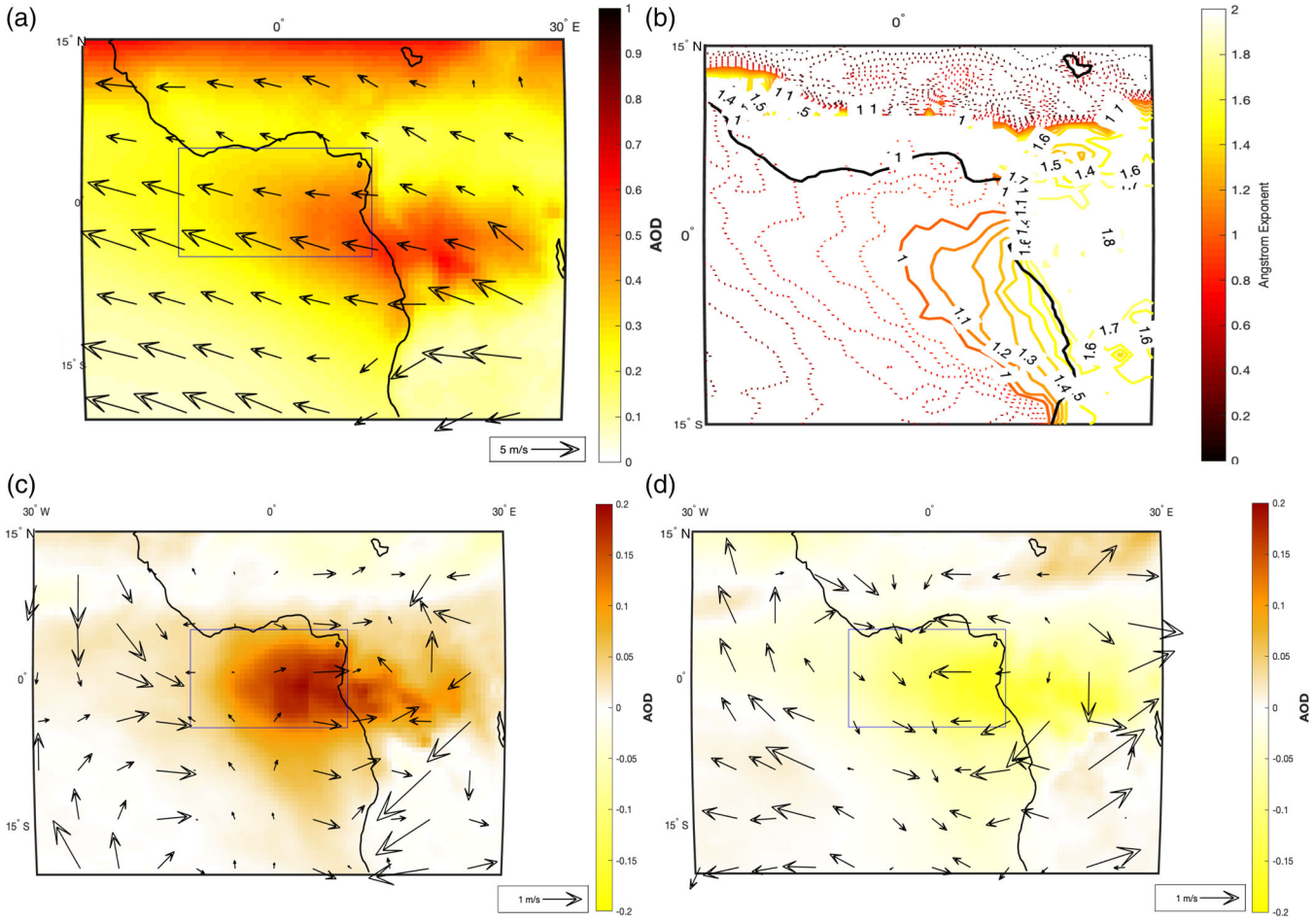

FIGURE 3 (a) Climatological AOD and 850 hPa winds. (b) Aerosol angstrom exponent for years 2013–2015. Contour interval is 0.1 with values larger than 1 represented as solid lines. AOD and 850 hPa wind anomalies for dirty (c, d) clean days during the same time period. Rectangular boxes in (a, c, d) represent averaging areas for composite analysis

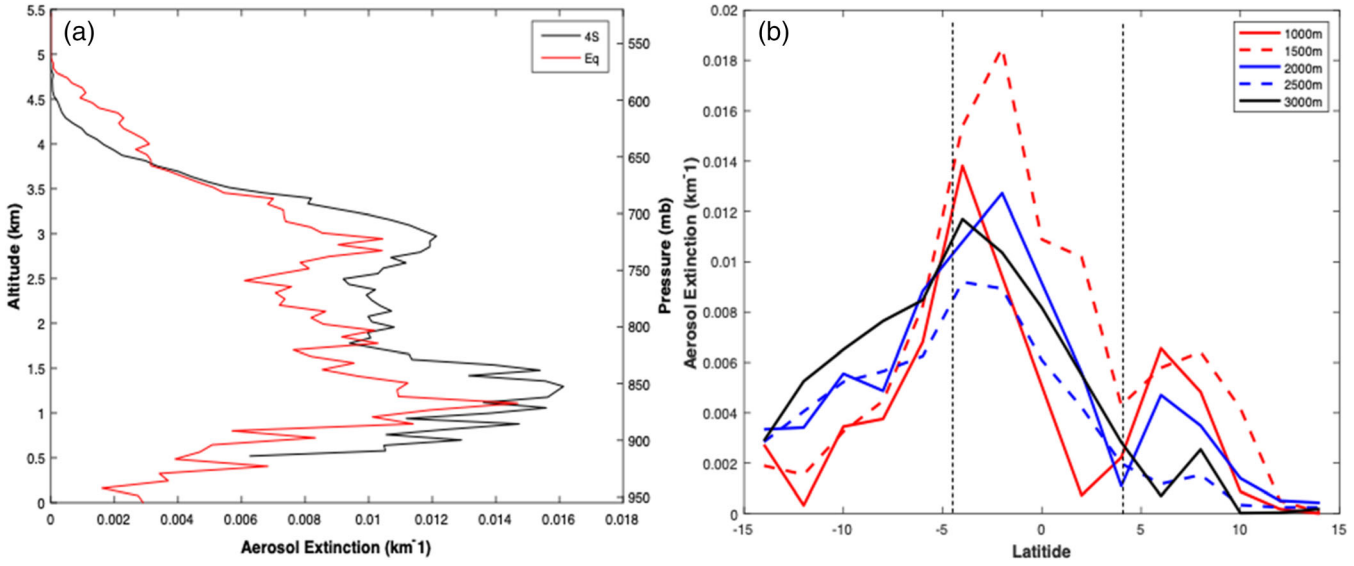

FIGURE 4 (a) Long-term mean vertical and (b) zonally averaged smoke aerosol extinction profiles derived from CALIOP for the month of June (2003–2015). Data in panel (a) represent values along the Prime Meridian. Dotted lines in panel (b) between 5°S and 4°N represent the boundary where AOD anomalies exceed 0.1. See Figure 1 for averaging area

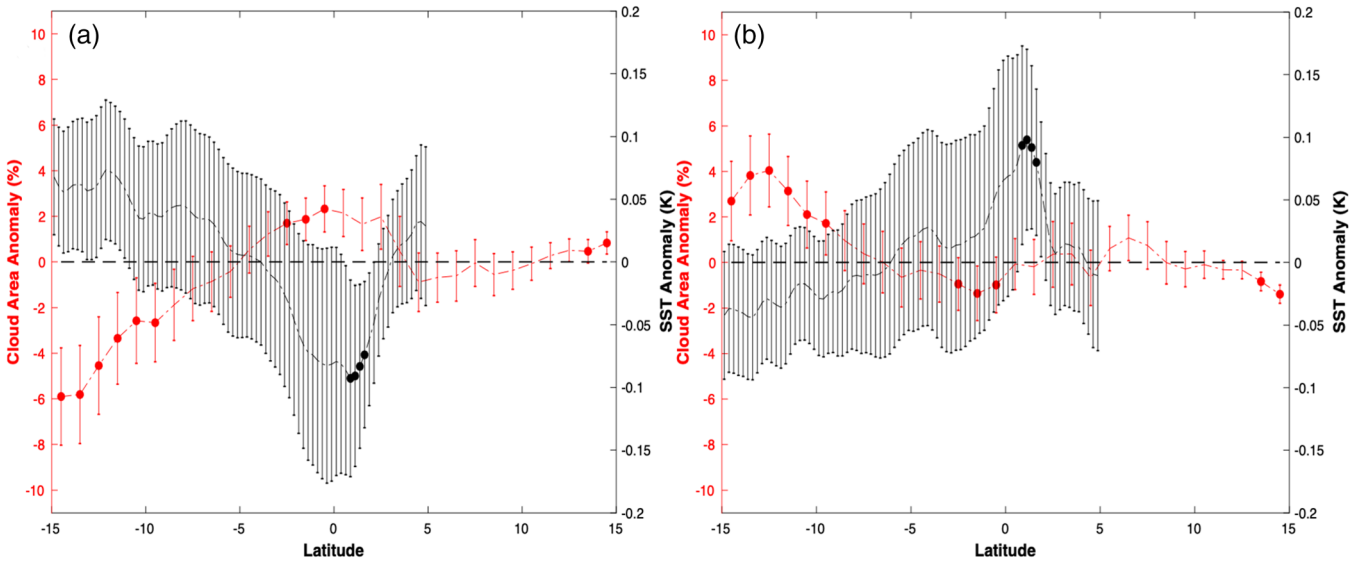

FIGURE 5 Zonally averaged low cloud area fraction and SST anomalies for (a) dirty and (b) clean smoke episodes. See Figure 1 for averaging area. Error bars range 1 standard error and filled circles represent locations where the difference between sampled means exceed the 95% confidence level

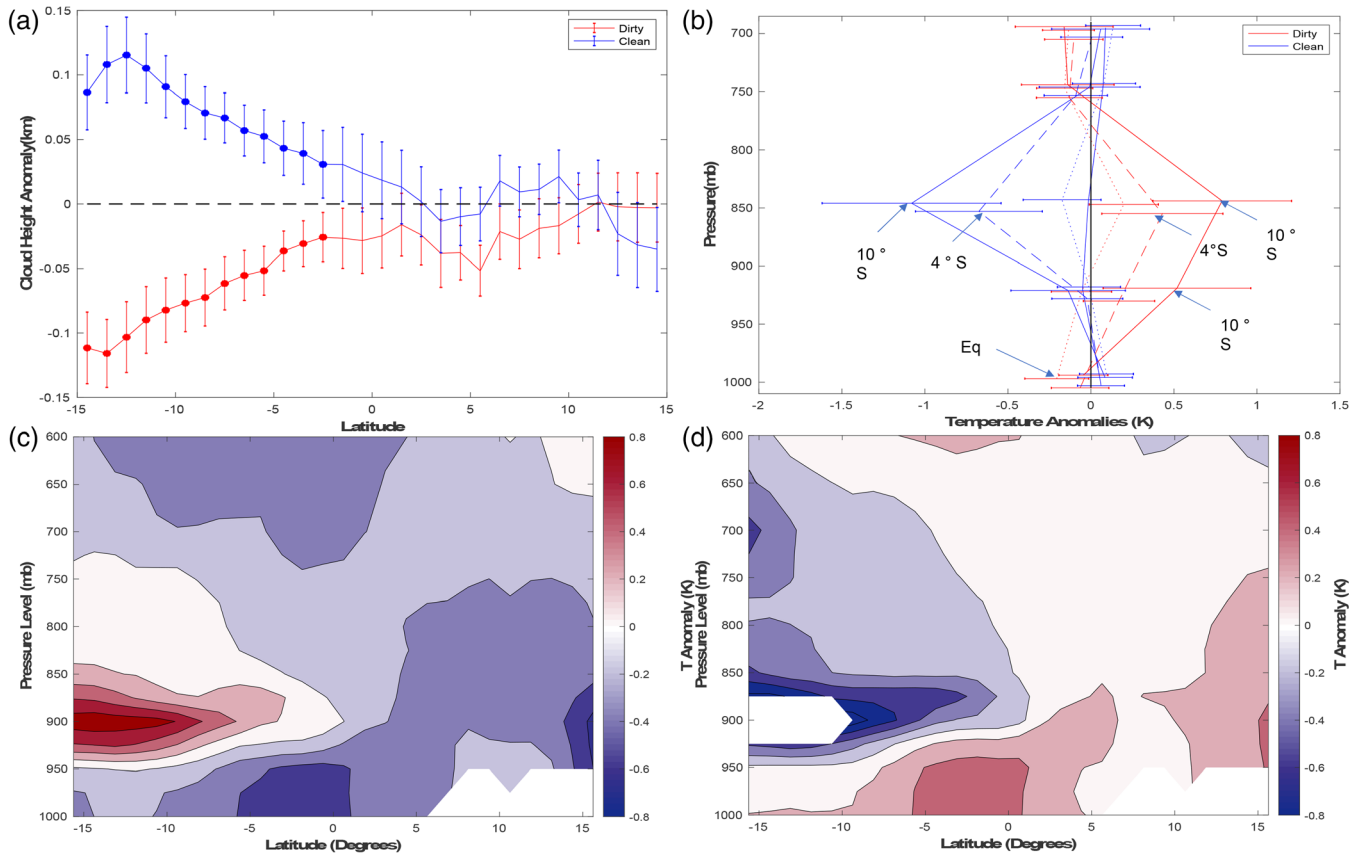

FIGURE 6 Anomalous changes in meteorological variables representing atmospheric stability and moisture: (a) cloud top height, (b) θ at various latitudes from ERA-Interim and temperature anomalies from MERRA-2 reanalysis for dirty (c) and clean (d) conditions. Data plotted in (b) are taken along the Prime Meridian. See Figure 1 for averaging area. Error bars range 1 standard error and filled circles represent locations where the difference between sampled means exceed the 95% confidence level. The arrows in (b) show the locations where θ anomalies are statistically significant

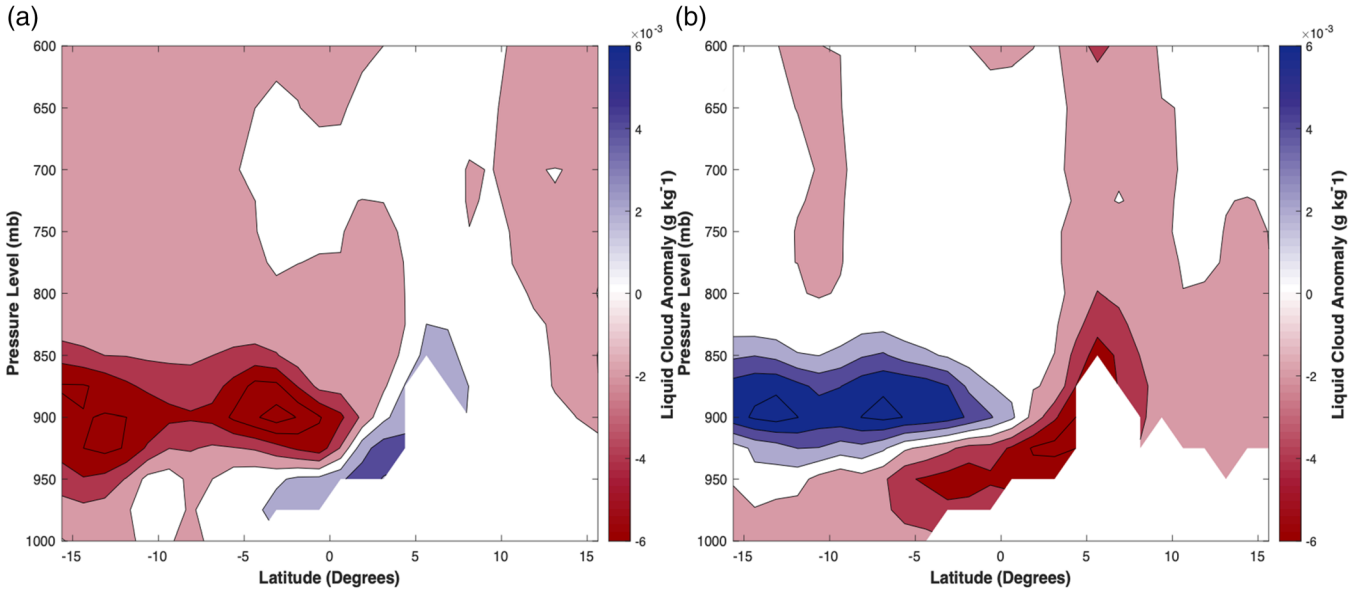

FIGURE 7 Anomalous changes in liquid cloud water content for dirty (a) and clean (b) conditions for the month of June

during dirty episodes, particularly at the equator where low cloud anomalies peak (Figures 5a and 6b,c). Our observed near-surface cooling also coincides with decreases in SST and coupled with warming within the stratocumulus deck (~900 hPa) leads to more stable conditions and reductions on cloud cover during dirty conditions (Figure 5a). With less biomass burning produced aerosols present, we find symmetrical responses opposite in sign. Particularly, a reduction in low-level cloud fraction within the cold tongue and positive SST anomalies in the GoG (Figure 5b). We also note favorable conditions for atmospheric instability near the cold tongue (Figure 6b,d).

Using a large eddy simulation (LES), Zhou *et al.* (2017) find a hastened SCT in time linked to increased dry air entrainment with the presence of absorbing aerosols. Their complementary experiments that included additional moisture aloft, which is believed to accompany biomass burning plumes relative to surrounding air (Adebiyi *et al.*, 2015), revealed similar results. In their study, absorbing aerosols above the cloud layer strengthens the inversion and reduces boundary layer height, in agreement with our findings. Additionally, as aerosols enter into the boundary layer, they find that enhanced entrainment of surrounding warm, dry air reduces cloud cover. During dirty aerosol conditions, we find increases in liquid cloud water amount within the GoG where we believe the boundary layer deepens and the SCT takes place (Figure 7a). Less liquid water amount is available within the GoG during clean conditions. In addition, increases in liquid water amount can be seen where stratocumulus decks dominate and extend well into the cold tongue.

4 | CONCLUSIONS

The individual impacts of biomass burning aerosols on LTS, low cloud cover and moisture availability culminate to shorten the SCT in space. Using observation and reanalysis data, we have isolated a mechanism for aerosol modulation on the SCT in the equatorial Atlantic that has not yet been discussed in the literature. This transition is located within the GoG and thus we conducted our AOD composite analysis at this location. Since previous research only looks at events with elevated smoke values, our results mainly focus on "dirty" days.

As smoke travels south of the GoG within the boundary layer, cloud fraction decreases (Figure 5a), as found in (Zuidema *et al.*, 2018), although they focus in a region slightly further south. Within the equatorial Atlantic (4°S–2°N), elevated smoke levels lead to increases (1–2%) in low cloud cover along with decreases in SST (~0.1 K) and potential temperature (~0.2 K) at the surface. Also, cloud top heights decrease 20–100 m, consistent with Deaconu *et al.* (2019). We attribute the switch from less low cloud for dirty conditions south of the cold tongue to more low clouds over the cold tongue to air–sea interactions unique to this region. In the subtropics, trade winds advect the boundary layer over increasing SSTs, which favors upward moisture flux from the surface to sustain cloud formations. Here, aerosol heating in the boundary

layer can cause the clouds to evaporate. In contrast, when the boundary layer reaches the cold tongue, the atmosphere develops near-surface stratification which cuts off the upward moisture flux needed to sustain clouds from dry air entrainment of the free troposphere (Mansbach and Norris, 2007). Here, it is possible that aerosol heating may increase stratification in the upper part of the boundary layer which would reduce dry air entrainment and lead to longer lasting cumulus clouds. Thus, our results are in agreement with Zhou *et al.* (2017) who find a hastened transition as a function of time as well as previous studies that find evidence of increased cloud fraction with enhanced loading (Wilcox, 2010; Wilcox, 2012; Li *et al.*, 2013) and increases in cloudiness when the vertical distance with the above aerosol layer is relatively small (Adebiyi and Zuidema, 2018).

Anomalous 850 hPa winds (Figure 3c,d) do not reflect a pattern that would control both aerosol and cloud structures, so we rule out the possibility of zonal wind variability causing such changes. During dirty conditions within the GoG, we find a stronger anticyclonic circulation associated with increased aerosols. Here, decreases in vertical velocity representing a more stable atmosphere limit dry air entrainment and as a result increases the moisture content as documented by Adebiyi *et al.* (2015). Changes in vertical velocity (Figure S1) intensity near the equator influences the subsidence portion of Hadley cell circulation. Weaker subsidence is also reflected through decreases in liquid cloud water (Figure 7a), cloud fraction (Figure 5a) and cloud top height (Figure 6a). Furthermore, reductions in cloud albedo can explain some of the increases in near-cloud temperature (Figure 6c) and feedback onto atmospheric stability.

We acknowledge that this research relies on remotely sensed observations and so may be subjected to uncertainties associated with satellite data, specifically the retrieval of clear-sky AOD, aerosol extinction coefficients and missing VIIRS data due to high cloud presence. Also, with such data, it is difficult to differentiate between mixed aerosol species (e.g., black carbon coated by sulfate). It is our hope that these findings will serve as a foundation for designing future field campaigns and testing modeling studies that investigate the SCT near the equatorial Atlantic.

ACKNOWLEDGEMENTS

This research forms a part of the PhD dissertation of OA, who was supported by a National Science Foundation Graduate Research (DGE-1650112), UC Dissertation Year and San Diego Foundation Fellowships. The National Science Foundation (OCE1419306 and OCE1600283) provided additional funding that supported this research.

ORCID

Osinachi F. Ajoku https://orcid.org/0000-0002-3973-471X

REFERENCES

Adebiyi, A.A. and Zuidema, P. (2018) Low cloud cover sensitivity to biomass-burning aerosols and meteorology over the southeast Atlantic. *Journal of Climate*, 31(11), 4329–4346.

Adebiyi, A.A., Zuidema, P. and Abel, S.J. (2015) The convolution of dynamics and moisture with the presence of shortwave absorbing aerosols over the southeast Atlantic. *Journal of Climate*, 28(5), 1997–2024.

Ajoku, O., Norris, J. and Miller, A.J. (2019) Observed monsoon precipitation suppression caused by anomalous interhemispheric aerosol. *Climate Dynamics*, 54, 1077–1091. https://doi.org/10.1007/s00382-019-05046-y.

Albrecht, B. (1989) Aerosols, cloud microphysics, and fractional cloudiness. *Science*, 245, 1227–1230. https://doi.org/10.1126/science.245.4923.1227.

Albrecht, B., Ghate, V., Mohrmann, J., Wood, R., Zuidema, P., Bretherton, C., Schwartz, C., Eloranta, E., Glienke, S., Donaher, S., Sarkar, M., McGibbon, J., Nugent, A.D., Shaw, R. A., Fugal, J., Minnis, P., Paliknoda, R., Lussier, L., Jensen, J., Vivekanandan, J., Ellis, S., Tsai, P., Rilling, R., Haggerty, J., Campos, T., Stell, M., Reeves, M., Beaton, S., Allison, J., Stossmeister, G. and Hall, S. (2019) Cloud system evolution in the trades (CSET): following the evolution of boundary layer cloud systems with the NSF–NCAR GV. *Bulletin of the American Meteorological Society*, 100(1), 93–121.

Albrecht, B.A., Bretherton, C.S., Johnson, D., Scubert, W.H. and Frisch, A.S. (1995) The Atlantic stratocumulus transition experiment—ASTEX. *Bulletin of the American Meteorological Society*, 76(6), 889–904.

Allen, R.J. and Ajoku, O. (2016) Future aerosol reductions and widening of the northern tropical belt. *Journal of Geophysical Research: Atmospheres*, 121, 6765–6786. https://doi.org/10.1002/2016JD024803.

Berrisford, P., Dee, D., Poli, P., Brugge, R., Fielding, K., Fuentes, M., Kallberg, P., Kobayashi, S., Uppala, S. & Simmons, A. (2011) *The ERA-Interim archive, version 2.0. ERA report series. 1. Technical Report. ECMWF pp23*. ECMWF.

Bretherton, C.S. (1992) A conceptual model of the stratocumulus-trade-cumulus transition in the subtropical oceans. In: *Proceedings of the 11th International Conference on International Commission on Clouds and Precipitation*, Vol. 1. Quebec, Canada: International Association of Meteorology and Atmospheric Physics Montreal, pp. 374–377.

Bretherton, C.S., Krueger, S.K., Wyant, M.C., Bechtold, P., Van Meijgaard, E., Stevens, B. and Teixeira, J. (1999) A GCSS boundary-layer cloud model intercomparison study of the first ASTEX Lagrangian experiment. *Boundary-Layer Meteorology*, 93(3), 341–380.

Bretherton, C.S. and Wyant, M.C. (1997) Moisture transport, lower-tropospheric stability, and decoupling of cloud-topped boundary layers. *Journal of the Atmospheric Sciences*, 54(1), 148–167.

Chung, D., Matheou, G. and Teixeira, J. (2012) Steady-state large-eddy simulations to study the stratocumulus to shallow

cumulus cloud transition. *Journal of the Atmospheric Sciences*, 69(11), 3264–3276.

Cochrane, S.P., Schmidt, K.S., Chen, H., Pilewskie, P., Kittelman, S., Redemann, J., LeBlanc, S., Pistone, K., Kacenelenbogen, M., Segal Rozenhaimer, M., Shinozuka, Y., Flynn, C., Platnick, S., Meyer, K., Ferrare, R., Burton, S., Hostetler, C., Howell, S., Freitag, S., Dobracki, A. and Doherty, S. (2019) Above-cloud aerosol radiative effects based on ORACLES 2016 and ORACLES 2017 aircraft experiments. *Atmospheric Measurement Techniques*, 12, 6505–6528. https://doi.org/10.5194/amt-12-6505-2019.

Deaconu, L.T., Ferlay, N., Waquet, F., Peers, F., Thieuleux, F. and Goloub, P. (2019) Satellite inference of water vapour and above-cloud aerosol combined effect on radiative budget and cloud-top processes in the southeastern Atlantic Ocean. *Atmospheric Chemistry and Physics*, 19(17), 11613–11634.

Diamond, M.S., Dobracki, A., Freitag, S., Small Griswold, J.D., Heikkila, A., Howell, S.G., Kacarab, M.E., Podolske, J.R., Saide, P.E. and Wood, R. (2018) Time-dependent entrainment of smoke presents an observational challenge for assessing aerosol–cloud interactions over the southeast Atlantic Ocean. *Atmospheric Chemistry and Physics*, 18(19), 14623–14636.

Ferek, R.J., Garrett, T., Hobbs, P.V., Strader, S., Johnson, D., Taylor, J.P., Nielsen, K., Ackerman, A.S., Kogan, Y., Liu, Q., Albrecht, B.A. and Babb, D. (2000) Drizzle suppression in ship tracks. *Journal of the Atmospheric Sciences*, 57(16), 2707–2728.

Ghan, S.J., Liu, X., Easter, R.C., Zaveri, R., Rasch, P.J., Yoon, J.H. and Eaton, B. (2012) Toward a minimal representation of aerosols in climate models: comparative decomposition of aerosol direct, semidirect, and indirect radiative forcing. *Journal of Climate*, 25(19), 6461–6476.

Hansen, J., Sato, M. and Ruedy, R. (1997) Radiative forcing and climate response. *Journal of Geophysical Research: Atmospheres*, 102(D6), 6831–6864.

Haywood, J. and Boucher, O. (2000) Estimates of the direct and indirect radiative forcing due to tropospheric aerosols: a review. *Reviews of Geophysics*, 38(4), 513–543.

Haywood, J.M., Abel, S.J., Barrett, P.A., Bellouin, N., Blyth, A., Bower, K.N., Brooks, M., Carslaw, K., Che, H., Coe, H., Cotterell, M.I., Crawford, I., Cui, Z., Davies, N., Dingley, B., Field, P., Formenti, P., Gordon, H., de Graaf, M., Herbert, R., Johnson, B., Jones, A.C., Langridge, J.M., Malavelle, F., Partridge, D.G., Peers, F., Redemann, J., Stier, P., Szpek, K., Taylor, J.W., Watson-Parris, D., Wood, R., Wu, H., and Zuidema, P. (2021) The CLoud–Aerosol–Radiation Interaction and Forcing: Year 2017 (CLARIFY-2017) measurement campaign. *Atmospheric Chemistry and Physics*, 21(2), 1049–1084. http://doi.org/10.5194/acp-21-1049-2021.

Johnson, B.T., Shine, K.P. and Forster, P.M. (2004) The semi-direct aerosol effect: impact of absorbing aerosols on marine stratocumulus. *Quarterly Journal of the Royal Meteorological Society*, 130, 1407–1422.

Klein, S.A. and Hartmann, D.L. (1993) The seasonal cycle of low stratiform clouds. *Journal of Climate*, 6(8), 1587–1606.

Li, J., von Salzen, K., Peng, Y., Zhang, H. and Liang, X.-Z. (2013) Evolution of black carbon semi-direct radiative effect in a climate model. *Journal of Geophysical Research: Atmospheres*, 118, 4715–4728. https://doi.org/10.1002/jgrd.50327.

Mansbach, D.K. and Norris, J.R. (2007) Low-level cloud variability over the equatorial cold tongue in observations and models. *Journal of Climate*, 20(8), 1555–1570.

Painemal, D., Kato, S. and Minnis, P. (2014) Boundary layer regulation in the southeast Atlantic cloud microphysics during the biomass burning season as seen by the A-train satellite constellation. *Journal of Geophysical Research: Atmospheres*, 119, 11288–11302. https://doi.org/10.1002/2014JD022182.

Painemal, D., Minnis, P. and Nordeen, M. (2015) Aerosol variability, synoptic-scale processes, and their link to the cloud microphysics over the northeast Pacific during MAGIC. *Journal of Geophysical Research: Atmospheres*, 120, 5122–5139. https://doi.org/10.1002/2015JD023175.

Pistone, K., Redemann, J., Doherty, S., Zuidema, P., Burton, S., Cairns, B., Cochrane, S., Ferrare, R., Flynn, C., Freitag, S., Howell, S.G., Kacenelenbogen, M., LeBlanc, S., Liu, X., Schmidt, K.S., Sedlacek III, A.J., Segal-Rozenhaimer, M., Shinozuka, Y., Stamnes, S., van Diedenhoven, B., Van Harten, G., and Xu, F. (2019) Intercomparison of biomass burning aerosol optical properties from in situ and remote-sensing instruments in ORACLES-2016. *Atmospheric Chemistry and Physics*, 19(14), 9181–9208. http://doi.org/10.5194/acp-19-9181-2019.

Ramanathan, V.C.P.J., Crutzen, P.J., Kiehl, J.T. and Rosenfeld, D. (2001) Aerosols, climate, and the hydrological cycle. *Science*, 294(5549), 2119–2124.

Reynolds, R.W., Smith, T.M., Liu, C., Chelton, D.B., Casey, K.S. and Schlax, M.G. (2007) Daily high-resolution-blended analyses for sea surface temperature. *Journal of Climate*, 20(22), 5473–5496.

Sandu, I. and Stevens, B. (2011) On the factors modulating the stratocumulus to cumulus transitions. *Journal of the Atmospheric Sciences*, 68(9), 1865–1881.

Sayer, A.M., Hsu, N.C., Bettenhausen, C., Lee, J., Kim, W.V. and Smirnov, A. (2018) Satellite Ocean Aerosol Retrieval (SOAR) algorithm extension to S-NPP VIIRS as part of the "Deep Blue" Aerosol Project. *Journal of Geophysical Research: Atmospheres*, 123, 380–400. https://doi.org/10.1002/2017JD027412.

Shinozuka, Y., Kacenelenbogen, M., Burton, S.P., Howell, S.G., Zuidema, P., Ferrare, R.A., LeBlanc, S.E., Pistone, K., Broccardo, S., Redemann, J., Schmidt, K.S., Cochrane, S.P., Fenn, M., Freitag, S., Dobracki, A., Segal-Rosenheimer, M., and Flynn, C.J. (2020) Daytime aerosol optical depth above low-level clouds is similar to that in adjacent clear skies at the same heights: airborne observation above the southeast Atlantic. *Atmospheric Chemistry and Physics*, 20(19), 11275–11285. http://doi.org/10.5194/acp-20-11275-2020.

Teixeira, J., Cardoso, S., Bonazzola, M., Cole, J., DelGenio, A., DeMott, C., Franklin, C., Hannay, C., Jakob, C., Jiao, Y., Karlsson, J., Kitagawa, H., Köhler, M., Kuwano-Yoshida, A., LeDrian, C., Li, J., Lock, A., Miller, M.J., Marquet, P., Martins, J., Mechoso, C.R., Meijgaard, E. v., Meinke, I., Miranda, P.M.A., Mironov, D., Neggers, R., Pan, H. L., Randall, D.A., Rasch, P.J., Rockel, B., Rossow, W.B., Ritter, B., Siebesma, A.P., Soares, P.M.M., Turk, F.J., Vaillancourt, P.A., Von Engeln, A., and Zhao, M. (2011) Tropical and subtropical cloud transitions in weather and climate prediction models: the GCSS/WGNE Pacific Cross-Section Intercomparison (GPCI). *Journal of Climate*, 24(20), 5223–5256. http://doi.org/10.1175/2011jcli3672.1.

Terai, C.R., Bretherton, C.S., Wood, R., Painter, G. (2014) Aircraft observations of aerosol, cloud, precipitation, and boundary layer properties in pockets of open cells over the southeast Pacific. *Atmospheric Chemistry and Physics*, 14(15), 8071–8088. http://doi.org/10.5194/acp-14-8071-2014.

Wilcox, E.M. (2010) Stratocumulus cloud thickening beneath layers of absorbing smoke aerosol. *Atmospheric Chemistry and Physics*, 10(23), 11769–11777. https://doi.org/10.5194/acp-10-11769-2010.

Wilcox, E.M. (2012) Direct and semi-direct radiative forcing of smoke aerosols over clouds. *Atmospheric Chemistry and Physics*, 12(1), 139–149. https://doi.org/10.5194/acp-12-139-2012.

Winker, D. (2015) *CALIPSO LID_L3_APro_AllSky-StandardHDF File – Version 3.00.* https://asdc.larc.nasa.gov/project/CALIPSO/CAL_LID_L3_APro_AllSky-Standard-V3-00_V3-00: NASA Langley Atmospheric Science Data Center DAAC. https://doi.org/10.5067/caliop/calipso/cal_lid_l3_apro_allsky-standard-v3-00.

Wood, R. and Bretherton, C.S. (2006) On the relationship between stratiform low cloud cover and lower-tropospheric stability. *Journal of Climate*, 19(24), 6425–6432.

Wood, R., Kuan-Ting, O, Bretherton, C.S., Mohrmann, J., Albrecht, B.A., Zuidema, P., Ghate, V., Schwartz, C., Eloranta, E., Glienke, S., Shaw, R.A., Fugal, J., and Minnis, P. (2018) Ultraclean layers and optically thin clouds in the stratocumulus-to-cumulus transition. Part I: observations. *Journal of the Atmospheric Sciences*, 75(5), 1631–1652. http://doi.org/10.1175/jas-d-17-0213.1.

Yamaguchi, T., Feingold, G. and Kazil, J. (2017) Stratocumulus to cumulus transition by drizzle. *Journal of Advances in Modeling Earth Systems*, 9, 2333–2349. https://doi.org/10.1002/2017MS001104.

Yamaguchi, T., Feingold, G., Kazil, J. and McComiskey, A. (2015) Stratocumulus to cumulus transition in the presence of elevated smoke layers. *Geophysical Research Letters*, 42, 10478–10485. https://doi.org/10.1002/2015GL066544.

Zhou, X., Ackerman, A.S., Fridlind, A.M., Wood, R. and Kollias, P. (2017) Impacts of solar-absorbing aerosol layers on the transition of stratocumulus to trade cumulus clouds. *Atmospheric Chemistry and Physics*, 17(20), 12725–12742.

Zhou, X., Kollias, P. and Lewis, E.R. (2015) Clouds, precipitation, and marine boundary layer structure during the MAGIC field campaign. *Journal of Climate*, 28(6), 2420–2442.

Zuidema, P., Redemann, J., Haywood, J., Wood, R., Piketh, S., Hipondoka, M. and Formenti, P. (2016) Smoke and clouds above the southeast Atlantic: upcoming field campaigns probe absorbing aerosol's impact on climate. *Bulletin of the American Meteorological Society*, 97(7), 1131–1135.

Zuidema, P., Sedlacek, A.J., III, Flynn, C., Springston, S., Delgadillo, R., Zhang, J., Aiken, A.C., Koontz, A. and Muradyan, P. (2018) The Ascension Island boundary layer in the remote southeast Atlantic is often smoky. *Geophysical Research Letters*, 45(9), 4456–4465.

SUPPORTING INFORMATION

Additional supporting information may be found online in the Supporting Information section at the end of this article.

How to cite this article: Ajoku OF, Miller AJ, Norris JR. Impacts of aerosols produced by biomass burning on the stratocumulus-to-cumulus transition in the equatorial Atlantic. *Atmos Sci Lett*. 2021;e1025. https://doi.org/10.1002/asl.1025